


## Research Article

# Dynamic Characteristics of Metro Trains under Rescue Conditions

Ruiming Zou <sup>1</sup>, Shihui Luo,<sup>2</sup> Weihua Ma,<sup>2</sup> and Qing Wu<sup>3</sup>

<sup>1</sup>College of Civil Aviation Safety Engineering, Civil Aviation Flight University of China, Guanghan 618307, China

<sup>2</sup>State Key Laboratory of Traction Power, Southwest Jiaotong University, Chengdu 610031, China

<sup>3</sup>Centre for Railway Engineering, Central Queensland University, Rockhampton 4701, Australia

Correspondence should be addressed to Ruiming Zou; [rmzou@outlook.com](mailto:rmzou@outlook.com)

Received 16 June 2020; Revised 19 October 2020; Accepted 26 October 2020; Published 7 November 2020

Academic Editor: Yi Bao

Copyright © 2020 Ruiming Zou et al. This is an open access article distributed under the Creative Commons Attribution License, which permits unrestricted use, distribution, and reproduction in any medium, provided the original work is properly cited.

In order to study the dynamic characteristics of metro train under rescue conditions, a detailed dynamic model with different train formations is established, taking into account the characteristics of wheel-rail contact, nonlinear characteristics of suspension components, and nonlinear hysteresis characteristics of the draft gear systems. To verify the accuracy of the simulation results, field tests are carried out and comparison is made between simulation and test results. Then, simulation analyses are conducted under the condition of AW0 rescues AW0, AW0 rescues AW3, and AW3 rescues AW3. Based on the simulation results, the longitudinal dynamic characteristics of the train under different rescue conditions are compared, and the influence of the longitudinal impulse on the dynamic performance of coupler and vehicle is analyzed. Finally, some suggestions are put forward to improve the draft gear as well as the rescue method.

## 1. Introduction

With the rapid development of urban rail transit, more and more metro trains are put into operation. By the end of the year 2018, 35 cities in China have built urban rail transit lines, totaling 5761.4 km, among which subway covered 4354.3 km, accounting for 75.6%. In densely populated cities like Beijing, Shanghai, and Guangzhou, metro systems have a considerable number of passengers to transport every day. Considering the particularity of its operation mode, the metro system is supposed not only to have trains of high reliability but also be equipped with emergency package dealing with train faults and emergency rescue capability of quickly towing the faulty train away from the field [1]. Usually, the faulty train can be towed or pushed to the workshop by a rescue train in the practice of fault rescue. As the faulty train provides neither traction force nor braking force, the longitudinal impulse may be caused when traction or braking is applied under rescue conditions, resulting in vehicle damage and even serious accidents. Recently, a metro company carried out a metro train rescue field test under the

condition of an empty loading train (denoted as AW0) towing a full loading train (denoted as AW3), and the coupler was damaged. In addition, derailment caused by braking under train rescue condition happened on several metro lines in China. These phenomena show that in-depth study on longitudinal dynamics of the metro train under train rescue condition is urgently needed and its running performance under rescue condition cannot be ignored.

Studies have been carried out on the longitudinal dynamics of trains for a long time [2]. However, most studies focus on heavy-haul trains [2–6]. The longitudinal dynamics of metro trains always fail to attract enough attention due to their short formation. But their research method is still worthy of reference. In general, the main course of the longitudinal impulse of a heavy-haul train is the unsynchronized behavior of the rolling stock due to signal transmission. In order to alleviate the longitudinal impulse of heavy-haul trains, the main measures studied at present include ① new technology development, for example, the development and application of ECP technology [7, 8], and ② optimization of existing equipment, such as the modeling

and optimization of the draft gear system [9, 10], as well as the air brake systems [11]. On the other side, lots of longitudinal train dynamics simulators are developed [12, 13]. All the above measures and technologies have greatly improved the development of heavy-haul transportations. Compared with freight trains, passenger trains have relatively shorter train formation; therefore, the longitudinal impulse of passenger trains mainly affects the ride quality of passengers [14] and has relatively insignificant influence on the safety under normal operating conditions. However, its longitudinal dynamics will be seriously worsened under rescue conditions [15].

To simplify the calculation and increase efficiency, generally, only the longitudinal DOF of the train is taken into consideration in the longitudinal dynamics researches of a heavy-haul train [16]. However, the recent study that indicated that the longitudinal dynamics of the train exerted a certain impact on the lateral and vertical dynamics of locomotives is worth noting, which was mainly attributed to the dynamic behavior of the coupler [17–19]. For example, coupler deflection under compressive forces will produce a certain lateral component of the in-train forces, and the effect of the lateral force on the wheel-rail relationship will have a negative impact on the running safety of the train. Wei's research also suggested that vertical coupler force led to car body pitch and wheel load reduction, which resulted in local structural damage and vehicle movement interference [15].

In view of what we mentioned previously, this paper believes that it is essential to further consider the effect of the dynamic behavior of the coupler systems on the lateral and vertical dynamics performance when researching the running safety of metro trains under rescue conditions. Thus, 3D dynamic models of metro trains in different formations are built up, considering not only the wheel-rail contact and nonlinear characteristics of suspension components but also the deflection behavior of the coupler and nonlinear hysteresis characteristics of the draft gear systems. Then, the dynamic characteristics of the metro train under pushing and towing rescue modes are analyzed by the simulation method.

## 2. Metro Train Rescue Model

The dynamics models of the metro train are established based on its design parameters by using Simpack: rotary arm positioning is used on the primary suspension system of bogies, along with a primary vertical damper; secondary suspension system consists of two air springs, one lateral damper, two vertical dampers, and a lateral bump stop; besides, traction device and antirolling bar are also included. As for the motor system of the power bogie, rigid frame suspension is adopted, and, in order to simplify the dynamics model, the motor system is not regarded as an independent rigid body but is taken into account by incorporating its masses into bogie frame and wheelsets. On this basis, the vehicle dynamics model has 42 degrees of freedom. Then, a 3D metro train rescue model can be established by the substructure method, and the vehicle

models are connected to each other by an automatic coupler model. The final train dynamics model has 504 degrees of freedom in total. The DOF of each rigid body component is shown in Table 1. In order to reflect the dynamic responses of the metro train more objectively, the characteristics of wheel-rail contact, nonlinear characteristics of suspension components, and nonlinear hysteresis characteristics of the draft gear systems are taken into account in the dynamics model. Among them, FASTSIM algorithm is used to calculate the wheel/rail relationship. Relevant modeling parameters are shown in Table 2.

In normal operation, the metro train consists of two subunits as shown in Figure 1. As can be seen from the figure, a subunit of the metro train is composed of one vehicle with two motor bogies (denoted as M) and two vehicles with just one motor bogie (denoted as TMC). Therefore, the tractive force provided by vehicle TMC is only half of that by vehicle M. But the braking system is the same whether it is a trailer bogie or a motor bogie, so the braking forces of vehicle TMC and vehicle M are the same. The metro train will lose all power when it breaks down, so a rescue train is needed to tow it away. The rescue train and the faulty train are connected by the coupler to form a train that consists of 12 vehicles.

*2.1. Mathematical Model of Draft Gear.* The characteristics of draft gear have a great influence on the longitudinal dynamics of metro trains. The static impedance characteristics of the draft gear used by the metro train are shown in Figure 2. The maximum pulling stroke is 40 mm, while the maximum compression stroke is 50 mm; the loading path and the unloading path of the draft gear model are indicated by functions  $f_u(x)$  and  $f_l(x)$ , with stroke  $x$  as a variable. The impedance characteristics of the draft gear are composed of two parts: nonlinear stiffness characteristics and hysteresis characteristics.

Spring force  $f_k(x)$  under a particular stroke  $x$  can be defined as

$$f_k(x) = \frac{1}{2} [f_u(x) + f_l(x)]. \quad (1)$$

The hysteresis force  $f_{\text{hys}}(x)$  under a particular stroke  $x$  is given by

$$f_{\text{hys}}(x) = \frac{1}{2} [f_u(x) - f_l(x)]. \quad (2)$$

Draft gear force  $F_{\text{DG}}(x, \Delta v)$  can be described according to

$$F_{\text{DG}}(x, \Delta v) = f_k(x) + f_{\text{hys}}(x) \cdot \text{sign}(\Delta v \cdot x). \quad (3)$$

The working condition of the draft gear is determined by the arithmetic product of stroke  $x$  and the relative velocity  $\Delta v$ : when  $x \cdot \Delta v > 0$ , it can be determined that the draft gear is in the loading state, and the coupler force changes along with the curve  $f_u(x)$ ; when  $x \cdot \Delta v < 0$ , the draft gear is unloading, and the coupler force changes along with the

TABLE 1: DOF list of rigid body.

DOF	Longitudinal $x$	Lateral $y$	Vertical $z$	Roll $\alpha$	Pitch $\beta$	Yaw $\gamma$
Car body	√	√	√	√	√	√
Bogie frame	√	√	√	√	√	√
Wheelset	√	√	√	√	√	√
Coupler yoke	√					
Coupler					√	√

TABLE 2: Modeling parameters.

Major parameters	M		TMC	
	AW0	AW3	AW0	AW3
Wheel load (t)	10.03	15.8707	9.9165	15.6047
Wheel/rail	DIN 5573/China 60 kg rail			
Wheelbase (m)	2.5			
Distance between bogie centers (m)	15.7			
Wheel diameter (mm)	840			
Primary longitudinal stiffness (MN/m)	17			
Primary lateral stiffness (MN/m)	9			
Primary vertical stiffness (MN/m)	1.22			
Secondary horizontal stiffness (MN/m)	0.12	0.16	0.12	0.16
Secondary vertical stiffness (MN/m)	0.265	0.465	0.27	0.465
Secondary lateral bump stop clearance (mm)	15-15			
Height of coupler (mm)	660			
Horizontal angle of automatic coupler (°)	25			
Vertical angle of automatic coupler (°)	6			

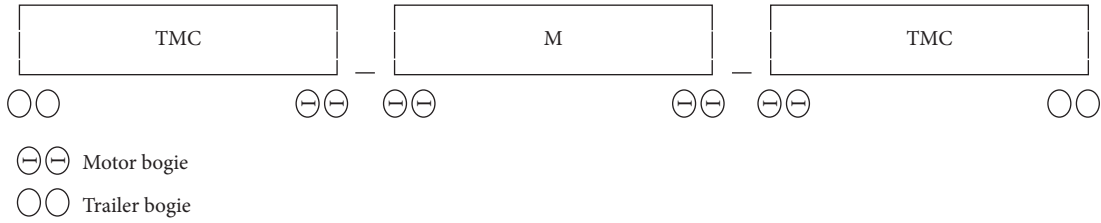


FIGURE 1: Subunit of metro train.

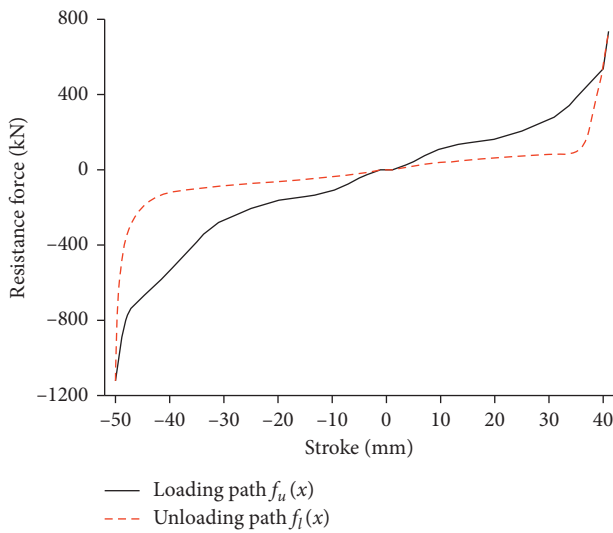


FIGURE 2: Draft gear characteristics.

curve  $f_l(x)$ . In order to avoid the unnecessary oscillation during the transition between loading state and unloading state, additional damping force  $f_{\text{damp}}$  is introduced and defined as follows [20]:

$$f_{\text{damp}}(\Delta v) = \begin{cases} -c_d \cdot \Delta v, & |f_l(x)| < |F_{\text{DG}}(x, \Delta v)| < |f_u(x)|, \\ 0, & \text{otherwise,} \end{cases} \quad (4)$$

where  $c_d$  is additional damping coefficient.

Coupler force  $F_{\text{coupler}}$  can be defined as the sum of draft gear force and additional damping force; thus the mathematical model of the coupler force can be obtained:

$$F_{\text{coupler}}(x, \Delta v) = F_{\text{DG}}(x, \Delta v) + f_{\text{damp}}(\Delta v). \quad (5)$$

**2.2. Running Resistance Force.** When running on the track, the metro train is subjected to resistance from many aspects, including vehicle weight, size, speed, type of bearing and its

application status, wheel-rail status, and wind resistance, so it is very difficult to accomplish a precise calculation of running resistance through a mathematical model. Because of this, the empirical formula is taken to describe the resistance per unit during the running process:

$$w_0 = a + bv + cv^2, \quad (6)$$

where  $w_0$  is the resistance per unit of the metro train;  $v$  is the velocity of the metro train; the value of each coefficient in the formula is shown in Table 3. In addition, the starting resistance per unit  $w_q$  is set at 49 N/t in the calculation.

**2.3. Tractive Force and Braking Force.** According to the design parameters of the metro train, the starting traction of AW0 status is 18.5 kN per power wheelset under the conditions of semiworn wheels and contact voltage at DC1500 V. Besides, the additional tractive force of 25 kN per power wheelset can be achieved via high acceleration/rescue switch, yet the requirement on the adhesive coefficient is higher. Since the available adhesion between the wheel and rail in the AW3 status is higher, the starting traction of AW3 can be directly up to 400 kN.

Emergency braking is one of the methods employed to stop the train as soon as possible in the case of emergency, but the longitudinal impulse generated by emergency braking is more prominent. Due to the consideration of safety and reliability, emergency braking is totally dependent on pneumatic braking. The braking force provided by one bogie can be calculated according to

$$F_{EB} = n_s F_B \mu \left( \frac{R_b}{R_w} \right), \quad (7)$$

where  $F_{EB}$  is the braking force provided by one wheelset during braking;  $n_s$  is the number of brake disks of the wheelset;  $F_B$  is the pressure acting on the brake pad;  $R_b$  is the friction radius of the brake disk and  $R_w$  is the radius of the wheel;  $\mu$  is the dynamic friction coefficient between brake disk and brake pad; it can be calculated as follows:

$$\mu = 0.41 \frac{F_B + 2 \times 10^5}{4F_B + 2 \times 10^5} \cdot \frac{v + 150}{2v + 150}. \quad (8)$$

The pressure acting on the brake pad  $F_B$  is in proportion to the pneumatic pressure of brake cylinder  $P_c$ .  $F_B$  can be calculated according to

$$F_B = 10P_c A_p \gamma_z \eta_z - F_R \gamma_z \eta_z, \quad (9)$$

where  $P_c$  is pneumatic pressure of brake cylinder;  $A_p$  is effective area of piston in brake cylinder;  $\gamma_z$  is rigging ratio;  $\eta_z$  is efficiency factor and  $F_R$  is internal return force.

The parameters of the braking system are shown in Table 4.

TABLE 3: Coefficients of the formula concerning resistance per unit of metro train.

Status	$a$	$b$	$c$
AW0	26.7	0	0.004447
AW3	26.7	0	0.002629

TABLE 4: Parameters of braking system.

Parameters	Value	Unit
$P_c$ (max)	5.4	bar
$A_p$	142.7	cm <sup>2</sup>
$\gamma_z$	8.58	—
$\eta_z$	0.97	—
$F_R$	500	N
$R_b$	254	mm
$n_s$	2	—

**2.4. Verification of the Train Model.** In order to verify the correctness of the dynamics model, a comparison is made between simulation results and field test results. The field test was carried out on the line of Shanghai Metro maintenance facility. The test condition is AW0 rescues AW3 by pushing rescue mode. That is, AW3 is the faulty train, which is located in the front of driving direction, and AW0 is the rescue train, which is located in the rear of driving direction. The train accelerates from a standstill with different traction levels and applies emergency braking immediately when the speed reaches 5 km/h. Figure 3 shows the time history comparison of coupler force when the maximum tractive force is applied at 50%. It can be seen from the figure that both the test results and simulation results indicate that the coupler between the faulty train and the rescue train will suffer from compression force when the tractive force is applied, and there will be an obvious pulling impact between the two trains after the emergency braking is applied. At the same time, the test results and simulation results are close to each other in numerical value. Table 5 shows the comparison of the peak values of the coupler force between the rescue train and the faulty train with different traction levels. It is obvious in the table that there is little difference between simulation results and field test results, which proves the reliability of the dynamics model.

### 3. Simulation Analysis of Rescue Conditions

In order to investigate the dynamic responses of the metro train when different rescue methods are adopted, three kinds of train formation are analyzed in this paper: AW0 rescues AW0, AW0 rescues AW3, and AW3 rescues AW3. The track condition of all simulations is ideal straight track. The traction mode of the rescue train under all the conditions adopts the rescue mode, while faulty trains have no tractive force or braking force. Considering the particularity of the wheel-rail calculation, the initial speed of the model is set at 1 km/h, the train begins to

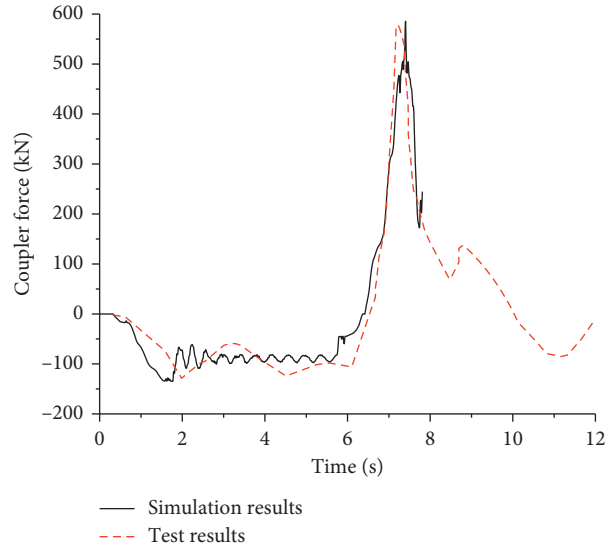


FIGURE 3: Time history of coupler force with 50% tractive force applied.

TABLE 5: Comparison between test results and simulation results.

Test condition	Test results (kN)		Simulation results (kN)		Margin of error	
	Pulling force	Compressive force	Pulling force	Compressive force	Pulling force	Compressive force
50% tractive force	590	-132	586	-125	0.7%	5.3%
60% tractive force	615	-162	611	-152	0.7%	6.2%
70% tractive force	650	-174	642	-169	1.2%	2.9%
80% tractive force	756	-188	739	-180	2.2%	4.3%

accelerate either through pushing or towing by the traction force of rescue train, and then the emergency braking is applied when the speed reaches 10 km/h. The longitudinal dynamic characteristics of the train and the dynamic responses of the vehicle are analyzed by simulation calculation.

### 3.1. Longitudinal Dynamics of the Train under Rescue Conditions

**3.1.1. AW0 Rescues AW0.** Figure 4(a) shows the maximum value of coupler forces when AW0 rescues AW0 (a positive value of coupler force indicates pulling force, while a negative value indicates compressive force, similarly hereinafter). As can be seen from the figure, the distributions of coupler forces under two rescue modes are almost symmetrical along the train, with both the maximum coupler forces at the coupler between two trains. The time history of coupler forces is shown in Figure 4(b). The rescue train is located at the rear of the train under the pushing rescue mode. As the faulty train has no braking ability, a great pulling impact has appeared when the emergency braking is applied, and the maximum pulling force on coupler reaches 659.9 kN. Meanwhile, under the towing rescue mode, the rescue train is located in front of the train, a great compressive impact would be more outstanding, and the maximum compressive force on coupler reaches 586.7 kN. Comparing the two maximum forces, it is obvious that the

numerical number under the towing rescue mode is slightly less than that under pushing rescue mode, which can be attributed to the inconsistency of pulling and compressive characteristics of the draft gear. Under the pulling condition, both the capacity and working stroke of the draft gear are smaller than those under compressive condition; therefore, draft gear cannot fully absorb the impact energy under pulling condition, which could lead to a rigid impact.

Figure 5 shows the distribution of the maximum longitudinal acceleration during emergency braking along the train. It can be seen from the distribution that, under two rescue modes, longitudinal accelerations are quite the opposite: under the pushing rescue mode, the longitudinal acceleration at the front position of the train is greater than that at the rear position; meanwhile, under the towing rescue mode, the longitudinal acceleration in the rear section is greater. In other words, the longitudinal acceleration of the faulty train is generally greater than that of the rescue train. Under the pushing rescue mode, the maximum longitudinal acceleration is observed in vehicle no. 3 at  $6.34 \text{ m/s}^2$ , while, under the towing rescue mode, it is observed at vehicle no. 10 at  $6.33 \text{ m/s}^2$ .

**3.1.2. AW0 Rescues AW3.** Figure 6(a) shows the distribution of the maximum coupler force along the train when AW0 rescues AW3 under pushing rescue mode and towing rescue mode, respectively. The maximum coupler forces when

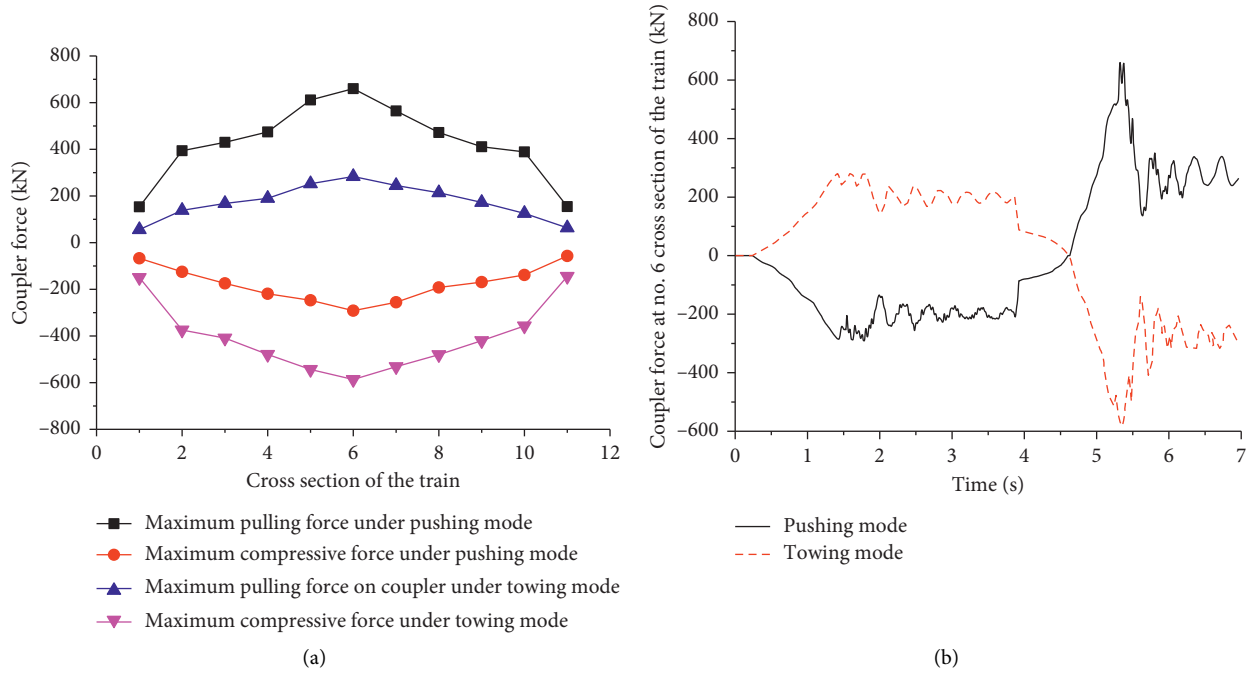


FIGURE 4: Coupler force when AW0 rescues AW0. (a) Maximum coupler forces. (b) Time history of coupler forces.

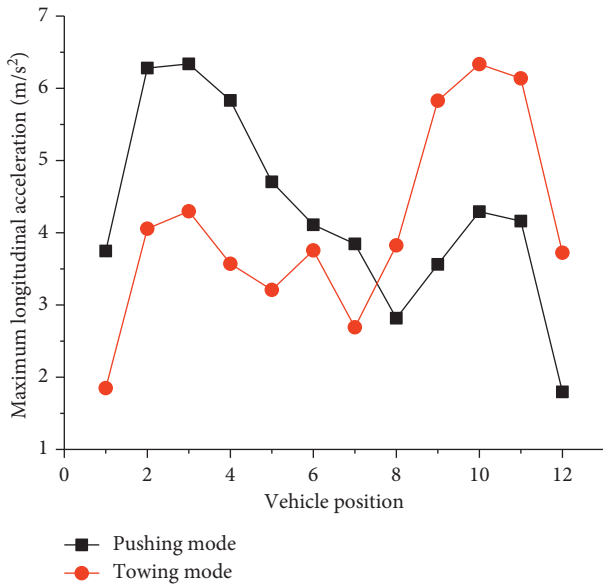


FIGURE 5: Maximum longitudinal acceleration when AW0 rescues AW0.

AW0 rescues AW3 increase compared with AW0 rescues AW0 as the mass of the faulty train increases. Besides, because the mass of the faulty train is larger than the rescue train, the in-train forces of the faulty train are greater than those of the rescue train. The maximum coupler forces are observed at the coupler between two trains. The time history of the coupler forces is shown in Figure 6(b), and the maximum coupler forces under the two rescue modes are shown in Table 6. It can be seen from the data that the coupler force during emergency braking in towing mode is

significantly reduced compared with that in pushing mode. It is apparent from Figure 7 that the longitudinal impulse caused by emergency braking under the pushing rescue mode leads to stroke exhaustion and results in a great rigid impact, which can easily cause damage to the vehicle or the coupler systems. As the draft gear has a relatively large compression capacity that can alleviate the compressive impact caused by emergency braking under the towing rescue mode and thus avoid the rigid impact effectively, the coupler force under the towing rescue mode is obviously smaller than that under the pushing rescue mode.

Figure 8 shows the distribution of the maximum longitudinal acceleration when AW0 rescues AW3. Due to the rigid impact under the pushing rescue mode, the longitudinal acceleration is greater than that under the towing rescue mode, and the values exceed the limit value of 9.81 m/s<sup>2</sup> at most of the vehicle positions. The maximum longitudinal accelerations under two rescue modes can be found in Table 6.

3.1.3. *AW3 Rescues AW3.* Figure 9(a) shows the distribution of the maximum coupler force when AW3 rescues AW3 under pushing rescue mode and towing rescue mode, respectively. As the masses of rescue train and faulty train are the same, the maximum coupler forces are almost symmetrical, and the maximum value can be found in Table 6. The time history of the coupler force between two trains is shown in Figure 9(b). The comparison shows that, due to the increase of braking force as well as train mass, the coupler force of AW3 rescues AW3 is significantly higher than that of AW0 rescues AW0. However, if the mass of rescue train increases while the emergency braking force remains unchanged, the equivalent force of the system is reduced

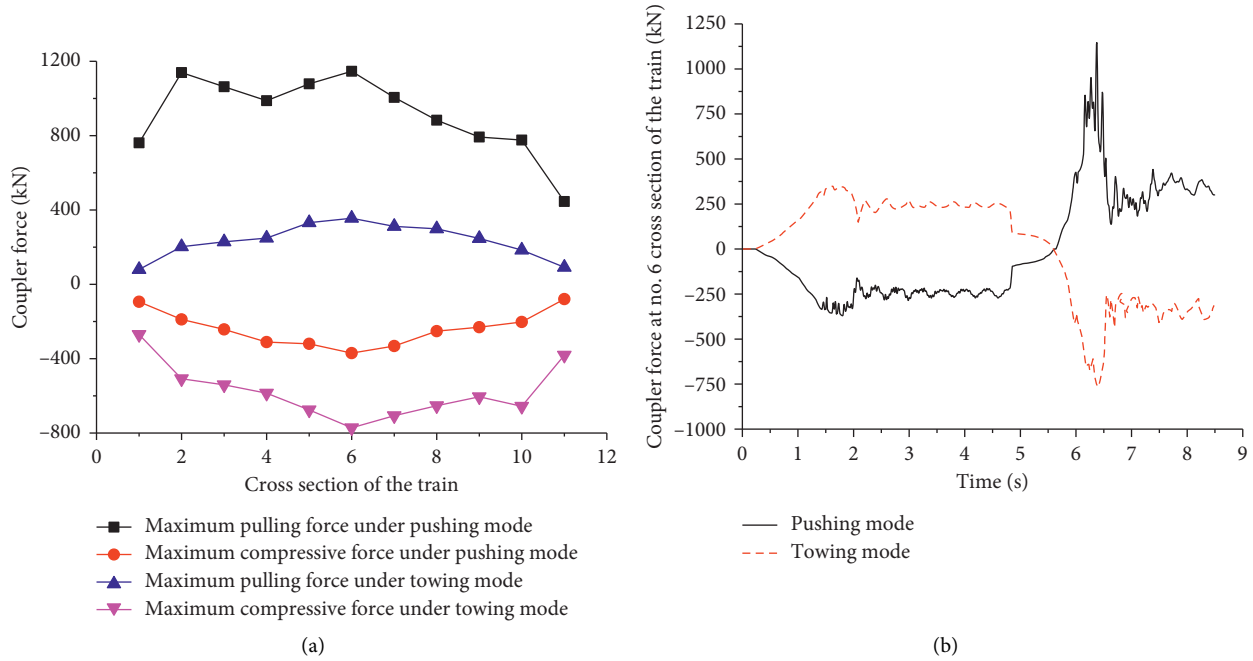


FIGURE 6: Coupler forces when AW0 rescues AW3. (a) Maximum coupler force. (b) Time history of coupler forces.

TABLE 6: Maximum values of longitudinal dynamics.

Rescue mode		AW0-AW0	AW0-AW3	AW3-AW3
Pushing mode	$F_{max}$	659.9 kN	1146.11 kN	1034.53 kN
	$A_{max}$	6.34 m/s <sup>2</sup>	14.82 m/s <sup>2</sup>	8.15 m/s <sup>2</sup>
Towing mode	$F_{max}$	586.7 kN	771.77 kN	716.9 kN
	$A_{max}$	6.33 m/s <sup>2</sup>	7.64 m/s <sup>2</sup>	5.51 m/s <sup>2</sup>

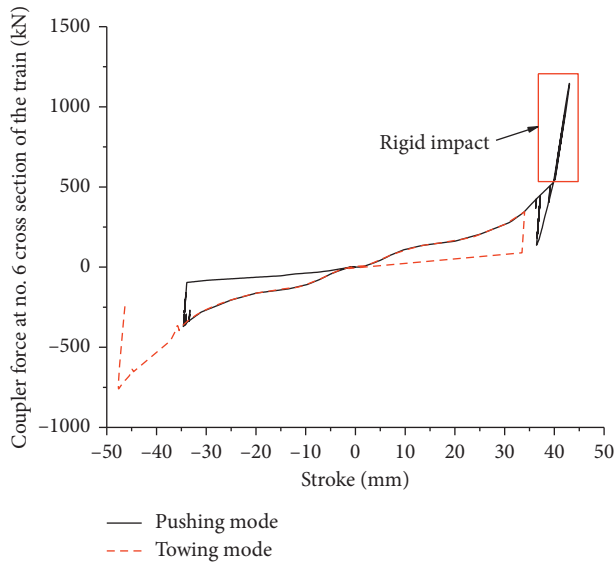


FIGURE 7: Dynamic response of the draft gear between two trains (AW0 rescues AW3).

although the equivalent mass of the system is increased. Therefore, the coupler force is smaller when AW3 rescues AW3 compared with the condition of AW0 rescues AW3.

Figure 10 shows the distribution of the maximum longitudinal acceleration when AW3 rescues AW3. The distribution still shows that the maximum longitudinal acceleration of the faulty train is greater than that of the rescue train. The corresponding maximum value is shown in Table 6.

**3.2. Effect of Longitudinal Impulse on Vehicle System Dynamics.** As the train is a multibody system with vehicles coupled to each other, the longitudinal dynamics of the train are also coupled with the lateral and vertical dynamics of the vehicle system through the coupler. Therefore, it is essential to conduct further analysis on the effect of longitudinal dynamics on the dynamic behavior of coupler systems and vehicle systems.

According to the foregoing calculation results, the maximum coupler force under rescue conditions is often seen at the coupler between two trains. So, in this part, vehicle no. 7 is taken as the research object to investigate the dynamic behavior of its front coupler and the effect of coupler behavior on the running safety of the vehicle. Generally, wheelset loading increase does not have much impact on the running safety of the train, but wheelset loading increase on one end of the coupler is surely accompanied by wheelset loading reduction on the other end due to the interaction of forces, so, considering the influence of coupler deflection randomness, the variation of wheelset

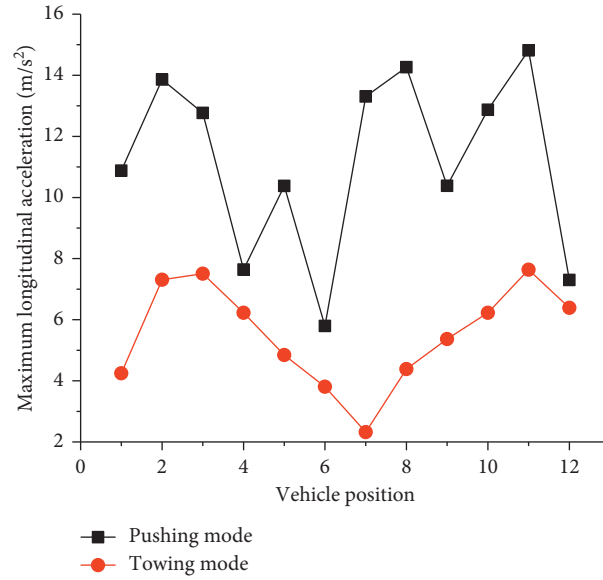


FIGURE 8: Maximum longitudinal acceleration when AW0 rescues AW3.

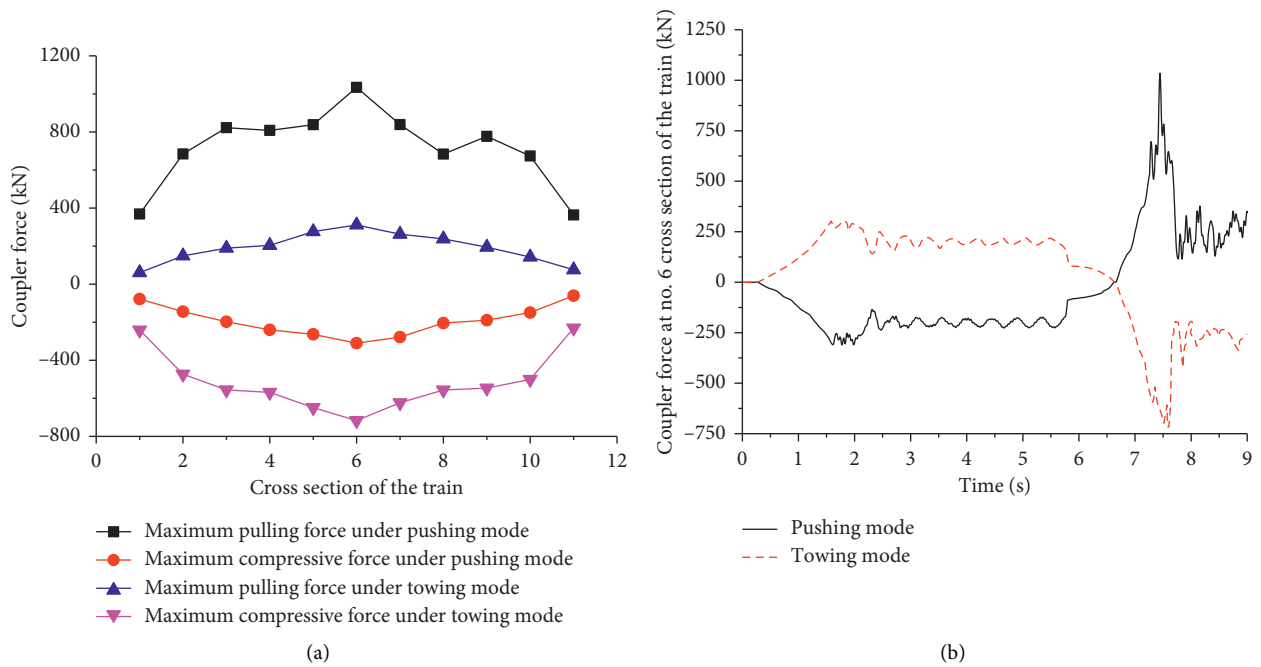


FIGURE 9: Coupler force when AW3 rescues AW3. (a) Maximum coupler forces. (b) Time history of coupler forces.

load has reference significance for vehicle running safety. The wheelset loading variation is defined as the difference between the wheelset vertical force and static load. It can be given by

$$\Delta P = P - P_{st}, \quad (10)$$

where  $\Delta P$  is the wheelset loading variation,  $P$  is the wheelset vertical force, and  $P_{st}$  is static wheelset load.

Figure 11 shows the dynamic behavior of the front coupler of vehicle no. 7 under various conditions. The numbers 0 and 3 in the figure represent AW0 and AW3,

respectively, while  $P$  and  $T$  represent pushing rescue mode and towing rescue mode, respectively. Along with the time history of coupler forces mentioned above, it can be found that its front coupler is subjected to compressive force during acceleration and then to pulling force after the application of emergency braking under pushing rescue mode, whereas, under towing rescue mode, it is quite the opposite. It also can be seen that the effect of the compressive force on the rotation behavior of the coupler is greater than that of the pulling force. The horizontal rotation angle of the coupler does not exceed  $3.5^\circ$  due to the physical restraint of the car body, while the vertical



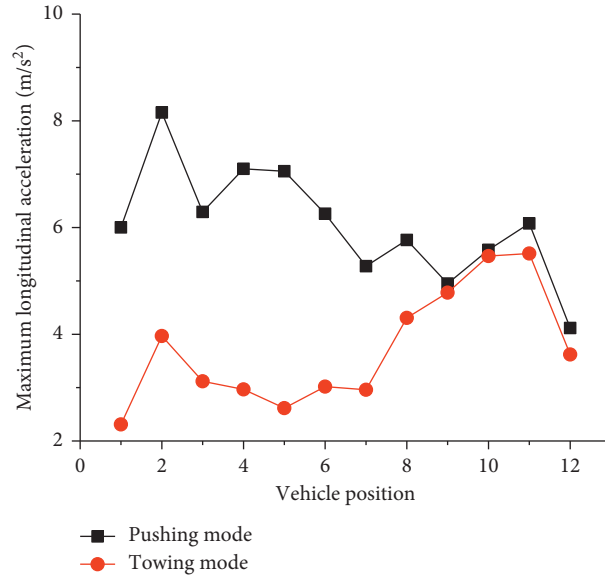


FIGURE 10: Maximum longitudinal acceleration when AW3 rescues AW3.

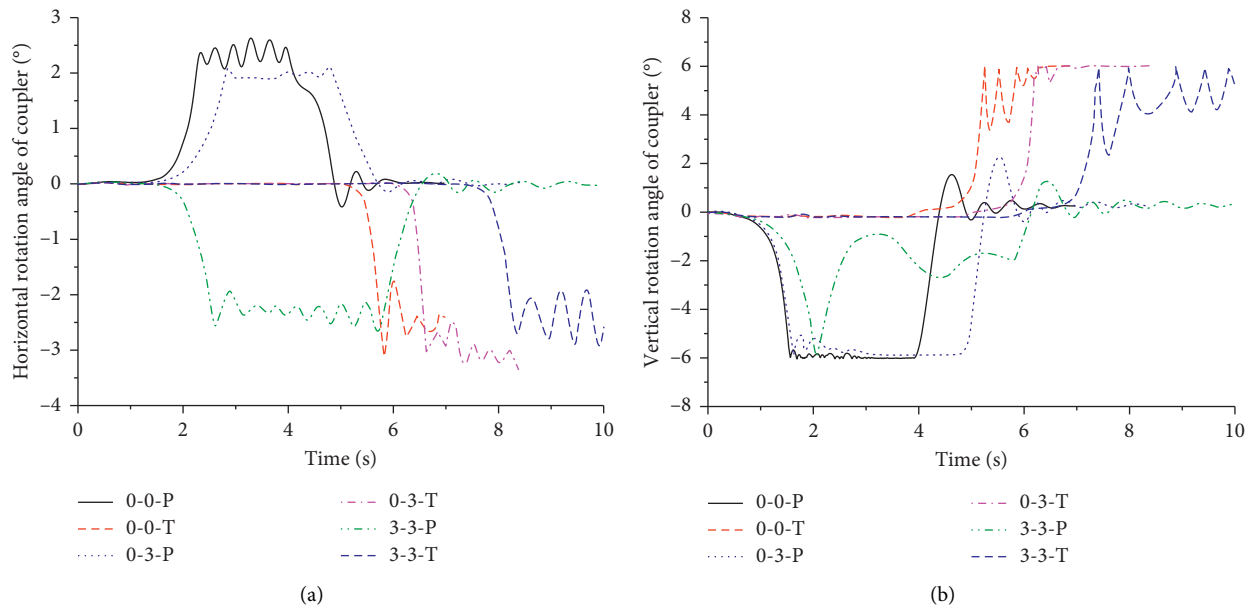


FIGURE 11: Coupler dynamic behavior. (a) Horizontal rotation angle. (b) Vertical rotation angle.

rotation angle deflects to the maximum angle allowed by its structure under the action of compressive force. The horizontal rotation of coupler leads to the generation of lateral force under the compressive status, which further causes the increase of wheelset lateral force. On the other hand, the vertical rotation angle of coupler leads to the generation of vertical force, which further causes the increase or reduction of wheelset load. Here, AW0 rescues AW0 is taken as the typical working condition to give the time history of the leading wheelset load of vehicle no. 7, as shown in Figure 12. Since the change rules of the wheelset load in other conditions are relatively similar, they will not be drawn here, but the maximum values in

each condition are shown in Table 7. As the longitudinal impulse under emergency braking condition is much greater than that under train starting condition, the maximum wheelset lateral force and maximum wheelset loading variation under pushing rescue mode are smaller.

#### 4. Optimization of Draft Gear

A comprehensive comparison of the above simulation results demonstrates that the longitudinal dynamic problem of the train is more prominent compared with the vehicle system dynamics when emergency braking is applied under metro rescue conditions. Due to the inconsistency of

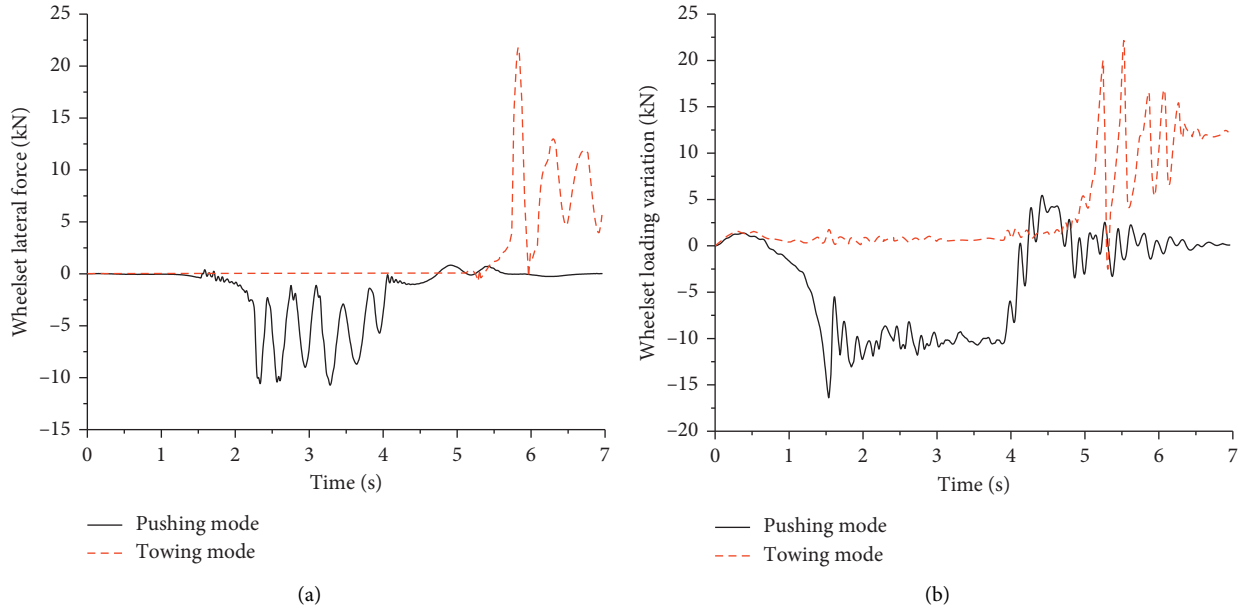


FIGURE 12: Vehicle dynamic responses when AW0 rescues AW0. (a) Wheelset lateral force. (b) Wheelset loading variation.

TABLE 7: Maximum values of wheelset load.

Rescue mode	Parameters	AW0-AW0 (kN)	AW0-AW3 (kN)	AW3-AW3 (kN)
Pushing mode	Wheelset lateral force	10.72	11.03	12.27
	Wheelset loading variation	16.40	19.27	21.32
Towing mode	Wheelset lateral force	22.09	22.78	19.71
	Wheelset loading variation	22.51	23.94	21.32

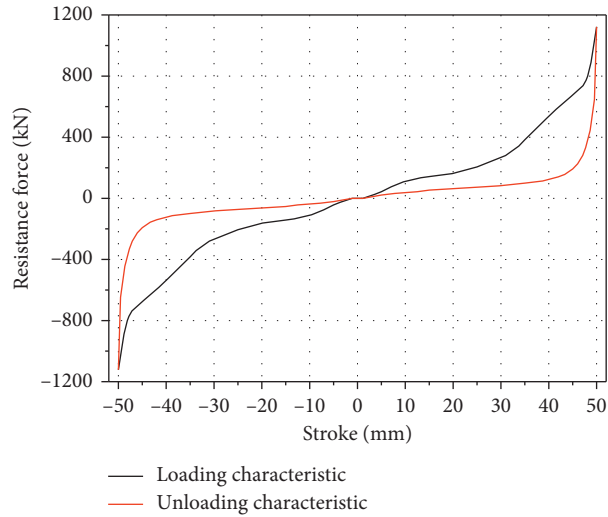


FIGURE 13: Optimized characteristics of draft gear.

compression capacity and pulling capacity of the draft gear, the severe rigid impact is generated under pushing rescue mode as the impact energy produced from emergency braking exceeds the pulling capacity of the draft gear. Besides, the coupler force has substantially surpassed the safety restriction zone allowed by its structure, which may easily cause the damage of vehicle parts. To solve this problem,

increasing the pulling capacity of the draft gear is proposed so as to alleviate the impact between rescue train and faulty train.

The pulling characteristics of the draft gear are modified to be consistent with the compression characteristics, as shown in Figure 13. The maximum coupler force and the maximum longitudinal acceleration when AW0 adopts

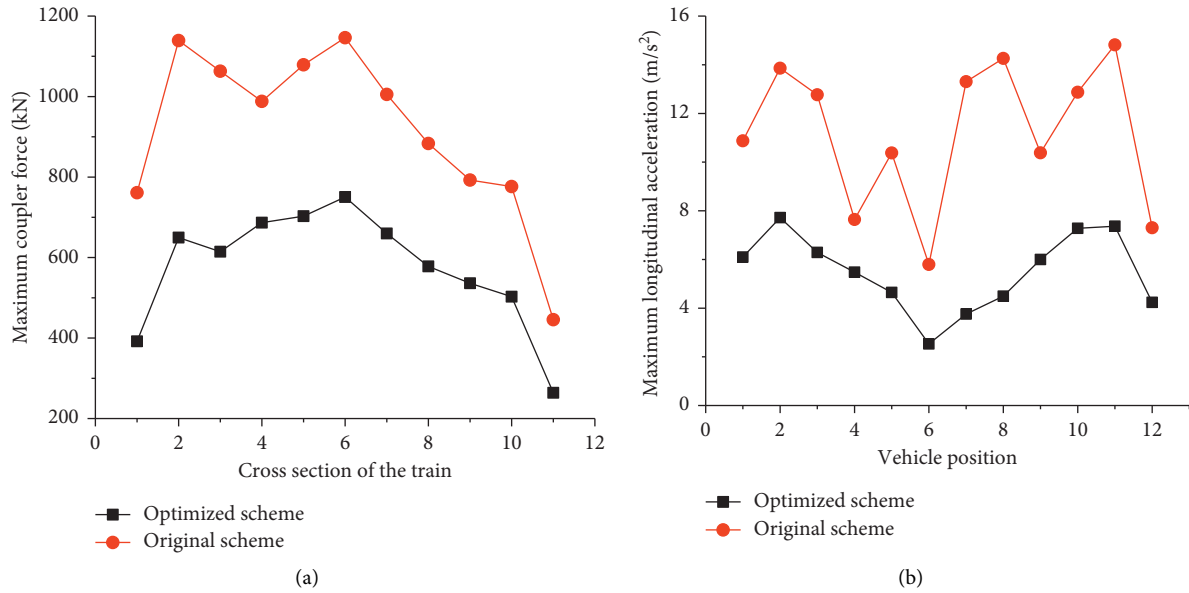


FIGURE 14: Results comparison of AW0 rescues AW3 before and after optimization. (a) Maximum coupler forces. (b) Maximum longitudinal acceleration.

pushing rescue mode to rescue AW3 can be obtained from simulation, as shown in Figure 14. Calculation results indicate that increasing the pulling capacity of the draft gear can significantly reduce the longitudinal impulse under pushing rescue mode. The maximum coupler force is reduced from 1146.11 kN to 750.37 kN, a decline of 34.53%; and the maximum longitudinal acceleration is reduced from 14.82 m/s<sup>2</sup> to 7.72 m/s<sup>2</sup>, a decline of 47.91%. Neither of the two indicators exceeds its corresponding limits; thus it can effectively reduce the possible damage of the coupler system as well as vehicle parts.

## 5. Conclusion

- (1) Due to the fact that faulty train has no traction or brake power, the longitudinal dynamics of a metro train under rescue conditions are prominent and deserve full attention. The maximum coupler force in the rescue mode is mostly at the connecting coupler of the rescue train and the fault train, and the maximum longitudinal acceleration of the vehicle in the fault train is generally higher than that of the rescue train. Optimizing the rescue mode and reducing the load on the train can effectively reduce the impact caused by braking.
- (2) The existing draft gear of the metro train has insufficient pulling capacity under rescue condition, so the emergency braking will lead to a rigid impact, which will cause the damage of components. So the capacity of draft gear should be fully considered during the design process. Increasing the pulling capacity of the draft gear can effectively reduce the longitudinal

impulse under pushing rescue mode, thus improving the force-bearing condition of the train.

- (3) The compressive in-train force can cause coupler rotation and generate corresponding lateral and vertical forces, resulting in a negative impact on the dynamic performance of the vehicle, which leads to the risk of derailment of the train. So how to restrain the rotation behavior of coupler under serious compression is also a problem worth thinking about.
- (4) In practice, it is recommended to evacuate passengers from the faulty train first, followed by AW0 rescue, and operate as smoothly as conditions permit, so as to reduce the longitudinal impulse of the train.

## Data Availability

The data used to support the findings of this study are available from the corresponding author upon request.

## Conflicts of Interest

The authors declare that they have no conflicts of interest.

## Authors' Contributions

Ruiming Zou conceived the study, established the dynamics model, carried out the simulations, and wrote the manuscript. Shihui Luo led the research thinking of the manuscript and revised the manuscript. Weihua Ma was

responsible for the data collection and analysis. Qing Wu provided guidance for the dynamics simulation and modeling and revised the manuscript.

## Acknowledgments

The authors acknowledge the support from the National Key R&D Program of China (Grant no. 2018YFC0809500) and the Sichuan Science and Technology Program (Grant no. 2018RZ0132). CRRC Zhuzhou Locomotive Co., Ltd., is highly appreciated for providing relevant parameters and test data for this paper.

## References

- [1] J. Y. Qi, "New vehicles and rescue of Beijing metro," *Urban Rapid Rail Transit*, vol. 21, no. 4, pp. 85–88, 2008.
- [2] Q. Wu, M. Spiriyagin, and C. Cole, "Longitudinal train dynamics: an overview," *Vehicle System Dynamics*, vol. 54, no. 12, pp. 1688–1714, 2016.
- [3] X. Zhuan and X. Xia, "Cruise control scheduling of heavy haul trains," *IEEE Transactions on Control Systems Technology*, vol. 14, no. 4, pp. 757–766, 2006.
- [4] M. Ansari, E. Esmailzadeh, and D. Younesian, "Longitudinal dynamics of freight trains," *International Journal of Heavy Vehicle Systems*, vol. 16, no. 1/2, pp. 102–131, 2009.
- [5] A. Nasr and S. Mohammadi, "The effects of train brake delay time on in-train forces," *Proceedings of the Institution of Mechanical Engineers, Part F: Journal of Rail and Rapid Transit*, vol. 224, no. 6, pp. 523–534, 2010.
- [6] R. Kovalev, A. Sakalo, V. Yazykov, A. Shamdani, R. Bowey, and C. Wakeling, "Simulation of longitudinal dynamics of a freight train operating through a car dumper," *Vehicle System Dynamics*, vol. 54, no. 6, pp. 707–722, 2016.
- [7] Y. Yang, L. Xiong, W. Liu, K. Gao, and Z. Huang, "An energy-based nonlinear pressure observer for fast and precise braking force control of the ECP brake," *International Journal of Precision Engineering and Manufacturing*, vol. 19, no. 10, pp. 1437–1445, 2018.
- [8] M. Chou, X. Xia, and C. Kayser, "Modelling and model validation of heavy-haul trains equipped with electronically controlled pneumatic brake systems," *Control Engineering Practice*, vol. 15, no. 4, pp. 501–509, 2007.
- [9] Q. Wu, S. Luo, T. Qu, and X. Yang, "Comparisons of draft gear damping mechanisms," *Vehicle System Dynamics*, vol. 55, no. 4, pp. 501–516, 2017.
- [10] C. Lei, J. Liu, L. Dong, and W. Ma, "Influence of draft gear modeling on dynamics simulation for heavy-haul train," *Shock and Vibration*, vol. 2019, Article ID 2547318, 11 pages, 2019.
- [11] W. Wei and Y. Lin, "Simulation of a freight train brake system with 120 valves," *Proceedings of the Institution of Mechanical Engineers, Part F: Journal of Rail and Rapid Transit*, vol. 223, no. 1, pp. 85–92, 2009.
- [12] Q. Wu and C. Cole, "Computing schemes for longitudinal train dynamics: sequential, parallel and hybrid," *Journal of Computational and Nonlinear Dynamics*, vol. 10, no. 6, 2015.
- [13] M. Spiriyagin, Q. Wu, and C. Cole, "International benchmarking of longitudinal train dynamics simulators: benchmarking questions," *Vehicle System Dynamics*, vol. 55, no. 4, pp. 450–463, 2017.
- [14] S. K. Sharma and A. Kumar, "Impact of longitudinal train dynamics on train operations: a simulation-based study," *Journal of Vibration Engineering & Technologies*, vol. 6, no. 3, pp. 197–203, 2018.
- [15] L. Wei, B. Zheng, and J. Zeng, "Braking induced impact for train to train rescue," *Vehicle System Dynamics*, vol. 55, no. 4, pp. 480–500, 2017.
- [16] X. Ge, K. Wang, L. Guo, M. Yang, K. Lv, and W. Zhai, "Investigation on derailment of empty wagons of long freight train during dynamic braking," *Shock and Vibration*, vol. 2018, Article ID 2862143, 18 pages, 2018.
- [17] R. Zou, C. Cole, Q. Wu, S. Luo, and W. Ma, "Research on the compression stability mechanism and its optimisation of coupler with arc surface contact," *Vehicle System Dynamics*, vol. 58, 2019.
- [18] K. Lv, K. Wang, Z. Chen et al., "The effect of the secondary lateral stopper on the compressed stability of the couplers and running safety of the locomotives," *Proceedings of the Institution of Mechanical Engineers, Part F: Journal of Rail and Rapid Transit*, vol. 232, no. 3, pp. 851–862, 2018.
- [19] L. Guo and K. Wang, "Analysis of coupler jackknifing and its effect on locomotives on a tangent track," *Proceedings of the Institution of Mechanical Engineers, Part F: Journal of Rail and Rapid Transit*, vol. 232, no. 5, pp. 1559–1573, 2018.
- [20] S. L. Sun, F. Li, Y. H. Huang, Z. Y. Zhou, and J. J. Ding, "Research on longitudinal characteristics of vehicle shunting impact," *Journal of the China Railway Society*, vol. 36, no. 1, pp. 22–27, 2014.